Jarrett-Wilkins, C. N., Musgrave, R. A., Hailes, R. L. N., Harniman, R. L., Faul, C. F. J., & Manners, I. (2019). Linear and Branched Fiber-like Micelles from the Crystallization-Driven Self-Assembly of Heterobimetallic Block Copolymer Polyelectrolyte/Surfactant Complexes. *Macromolecules*, *52*(19), 7289-7300. https://doi.org/10.1021/acs.macromol.9b01370

Linear and Branched Fiber-like Micelles from the Crystallization-Driven Self-Assembly of Heterobimetallic Block Copolymer Polyelectrolyte/Surfactant Complexes

Charles N. Jarrett-Wilkins,[a] Rebecca A. Musgrave,[a] Rebekah L. N. Hailes,[a] Robert L. Harniman,[a] Charl F. J. Faul,[a] and Ian Manners*[a,b]*

a - School of Chemistry, University of Bristol, Cantock's Close, Bristol, BS8 1TS, United Kingdom

b- Department of Chemistry, University of Victoria, Victoria, BC V8W 3V6, Canada

KEYWORDS Self-assembly, block copolymer, polyelectrolyte, micelle

ABSTRACT The solution self-assembly of a heterobimetallic diblock copolymer with a crystallisable poly(ferrocenyldimethylsilane) (PFS) core-forming block and a corona-forming segment featuring a poly(cobaltoceniumethylene) (PCE) based polyelectrolyte/surfactant complex, **PFS$_{50}$-*b*-[PCE][AOT]$_{50}$** (AOT = bis(2-ethylhexyl) sulfosuccinate), has been explored.

Fiber-like micelles were formed in selective solvents for the Co block, presenting a corona in which every repeat unit bears a charge. We found that key features of the 1D morphologies were dependent on both the polarity of the solvent medium and temperature. In the most polar of the explored solvent media (*i*PrOH), seeded growth from 1D seeds of **PFS$_{50}$-*b*-P2VP$_{739}$** (P2VP = poly(2-vinylpyridine)) yielded tapered B-A-B triblock co-micelles, where the width of the terminal B region derived from PFS-*b*-[PCE][AOT]$_n$ reduced on moving from the interface with the seed to the micelle termini. In addition, ca. 30 % of the micelles featured branching to yield multiple terminal blocks. On reducing the polarity of the solvent medium by the addition of 20% THF, the tapering of the micelles was no longer apparent, and the degree of branching was substantially increased to ca. 100 % of the population. With increased amounts of THF (30 %) the degree of branching reduced dramatically to ca. 3 %. In the least polar medium investigated (1:10 *i*PrOH:EtOAc), linear triblock co-micelles formed in which the terminal blocks were of consistent diameter, with no evidence for tapering or branching. However, significant unsymmetric growth (i.e. a higher degree of growth from one seed terminus compared to the other) to give non-centrosymmetric A-B diblock co-micelles was detected. Post self-assembly modification by coronal counterion exchange to alter the chemistry and solubility of the corona was also possible.

Introduction

Crystallisation-driven self-assembly (CDSA) describes the self-assembly process of amphiphilic block copolymers (BCPs) with a crystallisable core-forming block in selective solvents into 1D fibers and 2D platelets with a crystalline core.[1-13] By employing a seeded growth mechanism[3, 5, 14-17] it is possible to control the length of the micelles in an ambient or near ambient temperature process termed 'living' CDSA that is analogous to living covalent polymerisations of molecular monomers, which is not possible for analogous micelles with amorphous cores.[18] Key to the ability

to control the length of the self-assembled structures is that added, molecularly dissolved BCP (termed unimer) can grow epitaxially from the crystal faces at the termini of the micelles. The CDSA of BCPs containing PFS as a crystalline core-forming block has been extensively studied[19] and the seeded growth of these BCPs provides the possibility of forming complex architectures such as block co-micelles,[3, 14, 20] branched micelles[21-22] and two-dimensional platelets.[17, 23-24] Dynamic exchange of the individual BCP molecules between micelles is not detected at ambient temperatures, a feature promoted by crystallisation within the core, which kinetically traps the structures. This kinetic trapping is significant as it means that the dispersity does not increase over time. It is necessary for the corona-forming block to be well-solvated in the selective solvent to provide colloidal stability to the micelle. In addition, this block can be chosen to incorporate a range of different functionalities as long as it remains well solvated in the solvent system employed. For example, it is possible to form micelles with coronas that have hydrogen-bonding capabilities,[25] pendant fluorescent dyes,[26] and ligands which bind nanoparticles.[27] Living CDSA can also be performed with an expanding range of crystallisable core-forming blocks including π-conjugated or biodegradable materials.[5, 28-31]

In 2009 our group reported the thermal ring-opening polymerisation (ROP) of a strained dicarba[2]cobaltocenophane monomer to yield high molar mass neutral poly(cobaltocenylethylene) (PCE), which features neutral cobaltocene units in the main chain of the polymer (Fig. 1).[32] Upon one-electron oxidation of the cobaltocene units, poly(cobaltoceniumethylene), $[PCE][X]_n$ is formed, which is air- and moisture-stable with a variety of counter-anions (X = Cl, NO_3, OTf (OTf = trifluoromethanesulfonate), Fig. 1).[32-33] Cobalt-containing polymers are the subject of much current interest as a result of their attractive properties and potential biomedical applications.[34-42] Cobaltocenium-containing polymers in

which the metallocene is located in a pendent side group have been recently shown to inhibit the activity of bacteria such as methicillin-resistant staphylococcus aureus (MRSA),[34] which is able to hydrolyse β-lactam antibiotics by producing β-lactamase enzymes.[43] The polymer acts as a macromolecular scaffold that protects β-lactam antibiotics from hydrolysis via electrostatic interactions, and also itself inhibits MRSA cells via membrane lysis by adsorption of the cationic polymer to the negatively charged MRSA cell wall.[43]

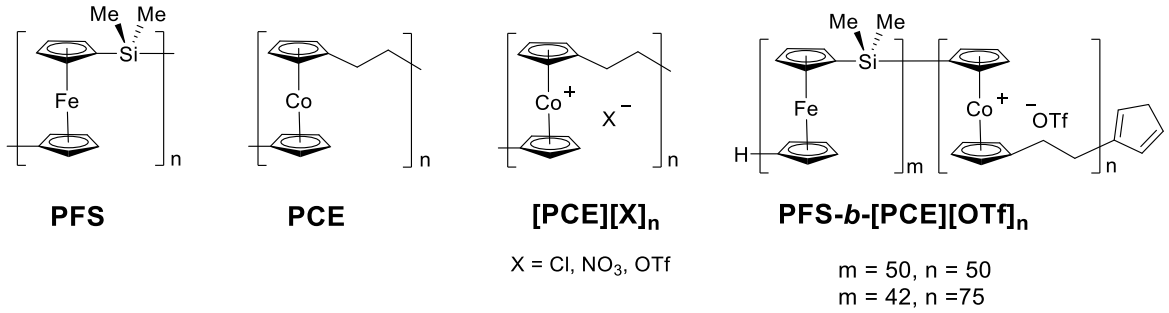

Figure 1. Metal-containing polymers poly(ferrocenyldimethylsilane) (PFS), poly(cobaltocenylethylene) (PCE), [poly(cobaltoceniumethylene)]$^{n+}$ ([PCE]$^{n+}$), and heterobimetallic BCP poly(ferrocenyldimethylsilane)-block-[poly(cobaltoceniumethylene)][triflate]$_n$ (**PFS$_m$-b-[PCE][OTf]$_n$**).

The cooperative assembly of charged surfactants and oppositely charged building blocks, termed 'ionic self-assembly', is an attractive method for forming functional hierarchically-ordered structures on the nanoscale.[44-48] Of particular interest is the cooperative electrostatic binding of surfactants to oppositely charged polyelectrolytes. This can drastically alter the solubility and properties of the polyelectrolyte, affording highly ordered supramolecular structures with unusual mechanical, optical, biological and electrical properties.[49] Previous work on PFS-based BCP

polyelectrolyte/surfactant complexes in the solid state has shown that the versatile ionic self-assembly route can lead to novel functional thin-film and bulk morphologies.[50-52]

We have previously shown that the two main-chain polymetallocenes, PFS and $[PCE]^{n+}$, can be covalently linked *via* photolytic ring-opening polymerisation to form poly(ferrocenyldimethylsilane)-*block*-[poly(cobaltoceniumethylene)][triflate]$_n$ (**PFS-*b*-[PCE][OTf]$_n$**) (Fig. 1).[53] This block metallopolymer is unusual for two main reasons. First, it features two main-chain metallocene-derived polymer blocks each based on different metals, and second, only one of these blocks ($[PCE]^{n+}$) is a polyelectrolyte, with the PFS block being uncharged. The solution self-assembly of PFS-*block*-polyelectrolyte materials is virtually unexplored and detailed studies are currently limited to materials in which the corona of PFS-based BCPs charge *via* the quaternisation of amino groups.[54-56] When 100% of the amino groups were quaternized, spherical micelles were formed in water.[54] However, in a separate study when between 1 and 3% of the corona was charged, platelet and scarf-like micelles formed.[55] The significant differences in self-assembly behavior of PFS-*block*-polyelectrolyte materials compared to neutral PFS-based BCPs likely arises as a result of: i) the enhanced difference in solubility between the two blocks,[53] ii) the dependence of the effective volume fraction of the corona on the chemical nature of the polyelectrolyte-anion segment, iii) the intra- and inter-coronal electrostatic interactions[57] and associated structural rigidity of the polyelectrolytic segment compared to neutral coronas.[58-59] Herein, we report studies of the seeded self-assembly of poly(ferrocenyldimethylsilane)-*block*-poly(cobaltoceniumethylene) materials that was enabled by replacement of the triflate counter ion of the polycobaltocenium block with a surfactant anion, which results in substantially increased solubility of the BCP in organic solvents.

Results

a) Synthesis and Characterization of PFS-*b*-[PCE][AOT]$_n$

The BCP **PFS$_{50}$-*b*-[PCE][OTf]$_{50}$** synthesized in our group in 2011 via a sequential photolytic ROP approach,[53] was found to be only sparingly soluble in tetrahydrofuran (THF). As a result, the solution self-assembly of this material was challenging to control, and small spherical micelles were observed in solvent mixtures chosen to be selective for the [PCE][OTf]$_n$ block.[53] In the presence of cylindrical seed micelles (composed of **PFS$_{34}$-*b*-P2VP$_{272}$** (P2VP = poly(2-vinylpyridine)), growth of **PFS$_{50}$-*b*-[PCE][OTf]$_{50}$** unimer was not only observed from the ends of the cylindrical seed, as is expected for epitaxial growth of BCPs with a crystallisable core, but was evident in three dimensions around the seed, as observed by transmission electron microscopy (TEM) and atomic force microscopy (AFM).[53, 60] This self-assembly behavior differed significantly with the living CDSA of reported neutral PFS-based BCPs, where epitaxial growth occurs from the active seed ends in 1D or 2D.[3] Due to the large difference in solubility of the neutral and polyelectrolytic blocks, it is expected that the unimer was poorly solvated and deposited very rapidly onto the seeds, forming kinetically trapped structures.

We surmised that counterion exchange of the triflate anion for a surfactant anion such as bis(2-ethylhexyl) sulfosuccinate (AOT) (Fig. 2a) would increase the solubility of the BCP in organic solvents and might aid self-assembly. We anticipated that this increased solubility should cause a slower rate of deposition of unimer onto the exposed crystal faces of the micelles during self-assembly and allow for better control over the micelle structure. In a 9:1 mixture of THF:methanol (MeOH), **PFS$_{50}$-*b*-[PCE][OTf]$_{50}$** was combined with 50 eq. of Na[AOT] and stirred for 24 h. Non-complexed surfactant and by-product Na[OTf] were removed via precipitation and washing with MeOH (see Supporting Information for details). ^{1}H DOSY NMR spectroscopy (Fig. S1) of the precipitated BCP product showed that the resonances arising from the [PCE]$^{n+}$ main chain and

those of the AOT surfactant exhibited the same diffusion coefficient, suggesting ion-pairing of the surfactant to the polyelectrolyte block in CD_2Cl_2. The **PFS_{50}-*b*-[PCE][AOT]$_{50}$** BCP was found to be readily soluble in THF (a marked increase relative to the triflate-paired starting material). DLS analysis confirmed that the material was molecularly dissolved, affording a well-defined peak with a hydrodynamic radius (R_h) of 7.5 nm and indicating negligible aggregation (Fig. S2). Attempted characterization by GPC in THF led to a single peak of relatively low dispersity (D = 1.20) with a molar mass lower than that expected (number-average molar mass M_n =10,570 $gmol^{-1}$ compared to a theoretical value of 43,950 $gmol^{-1}$) which suggested that partial dissociation of the AOT from the ion-pairs probably occurs in this solvent.

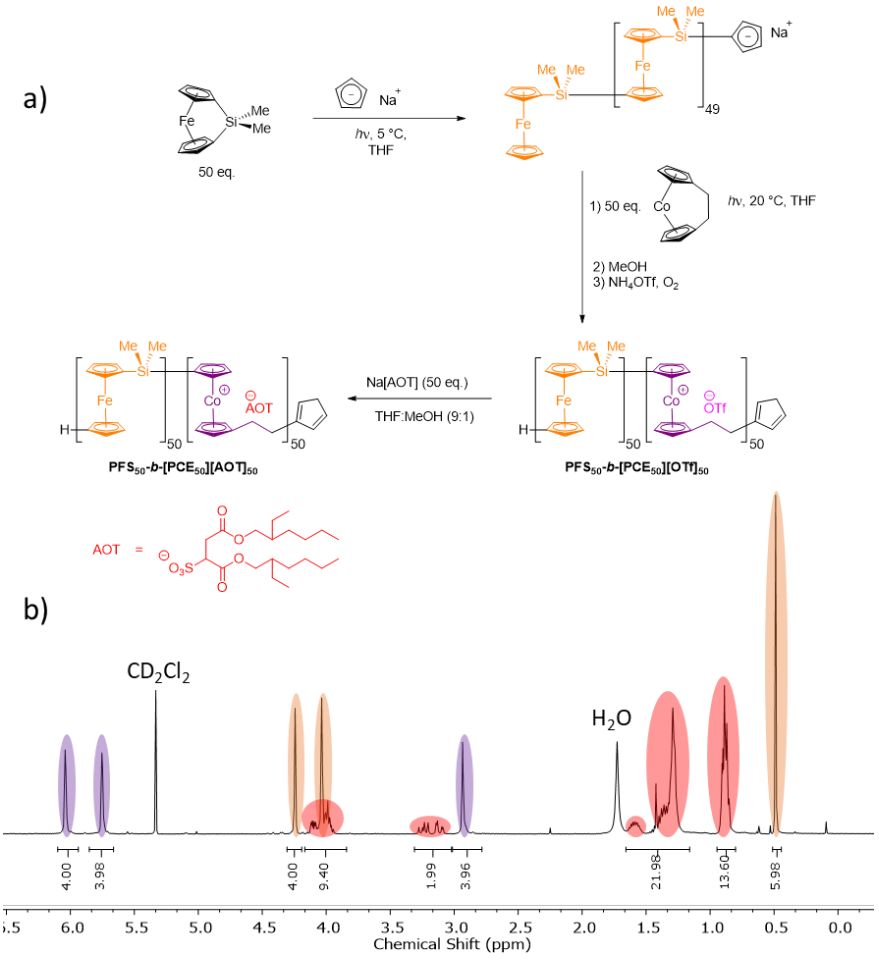

Figure 2. **(a)** Scheme showing the synthesis of **PFS$_{50}$-b-[PCE][OTf]$_{50}$** and exchange of the [PCE] counterion in the synthesis of **PFS$_{50}$-b-[PCE][AOT]$_{50}$** from **PFS$_{50}$-b-[PCE][OTf]$_{50}$**, **(b)** ^{1}H NMR of **PFS$_{50}$-b-[PCE][AOT]$_{50}$** in CD_2Cl_2.

b) Self-assembly in a highly polar medium (isopropanol)

Initially, a unimer solution of **PFS$_{50}$-*b*-[PCE][AOT]$_{50}$** in THF was added to **PFS$_{50}$-*b*-P2VP$_{739}$** seed micelles (L_n = 101 nm, L_w/L_n = 1.05) in isopropanol (*i*PrOH),[25] which is a good solvent for both P2VP and [PCE][AOT]$_n$, and a very poor solvent for PFS. The resulting solution was aged for 16 h and then drop-cast onto carbon-coated copper grids. Once the solvent had evaporated, the sample was studied by TEM. Analysis of TEM images revealed that the added **PFS$_{50}$-*b*-[PCE][AOT]$_{50}$** unimer had grown from the ends of the **PFS$_{50}$-*b*-P2VP$_{739}$** seeds producing BAB triblock co-micelles in which the width of the terminal block gradually decreased from the interface with the seed towards the end of the micelle, which we have termed a tapered morphology (Fig. S3 shows TEM images of micelles with a unimer:seed mass ratio of 5, 10 and 15 after ageing for 16 h). This growth differs significantly from the analogous self-assembly behavior of the original triflate-paired BCP **PFS$_{50}$-*b*-[PCE][OTf]$_{50}$**, which showed evidence of growth in all three dimensions around the seed micelle.[53]

Small spherical micelles, whose formation was attributed to the kinetic trapping of unimer BCP into aggregates with amorphous cores,[61-62] could also be observed by TEM after ageing the sample for 16 h (Fig. S3). In poor solvents for the core-forming block, rapid aggregation of this segment can occur to yield micelles with amorphous cores as there is insufficient time for the polymer chains to crystallize. Due to the relatively high molar mass of the core-forming blocks, even in the absence of core crystallinity, exchange of individual BCP molecules between aggregates and solution is slow and structural evolution to the thermodynamically preferred morphology can take

several months or longer, even infinitely long.[63] Upon ageing for several months, the spheres disappeared (Fig. 3a), presumably as BCP molecules evolve from the amorphous, kinetically-trapped assemblies to the thermodynamically preferred 1D micelles with crystalline cores. In addition, after ageing the sample for several months, a significant number of micelles featured branching points at a unimer:seed mass ratio of 15 (37%, Fig. 3a, see red circles).

The tapered nature of these micellar structures was further explored by AFM. The **PFS$_{50}$-*b*-P2VP$_{739}$** seeds had an average height of 19 nm and width of ca. 68 nm (Fig. 3d, red trace), although the latter value should be considered with caution as it is expected that the long P2VP corona makes a significant contribution to the width of the seeds in particular.[22] While the height of the terminal **PFS$_{50}$-*b*-[PCE][AOT]$_{50}$** blocks remained constant (ca. 10 nm; Fig. 3c and 3d, blue, green and purple traces), traversing the newly formed segment along the micelle axis away from the seed interface, the width decreased dramatically from ca. 72 nm to 24 nm by AFM, (Fig. 3d, blue, green and purple traces). Close to the interface with the seed, the width of the newly formed terminal block is significantly greater than the height, but at the termini of the triblock co-micelle the height and width were found to be of similar dimensions.

In general, for seeded growth of PFS BCPs, a linear relationship can be observed between the average length (L_n) of the micelles and the unimer:seed mass ratio, consistent with a living CDSA process.[14] In this case, it was difficult to quantify the increase in length of the micelles in *i*PrOH as a product of the unimer:seed mass ratio, due to the tapering and occasional branching. Qualitatively, as the unimer:seed mass ratio increased, longer micelles could be observed by TEM (Fig. S3).

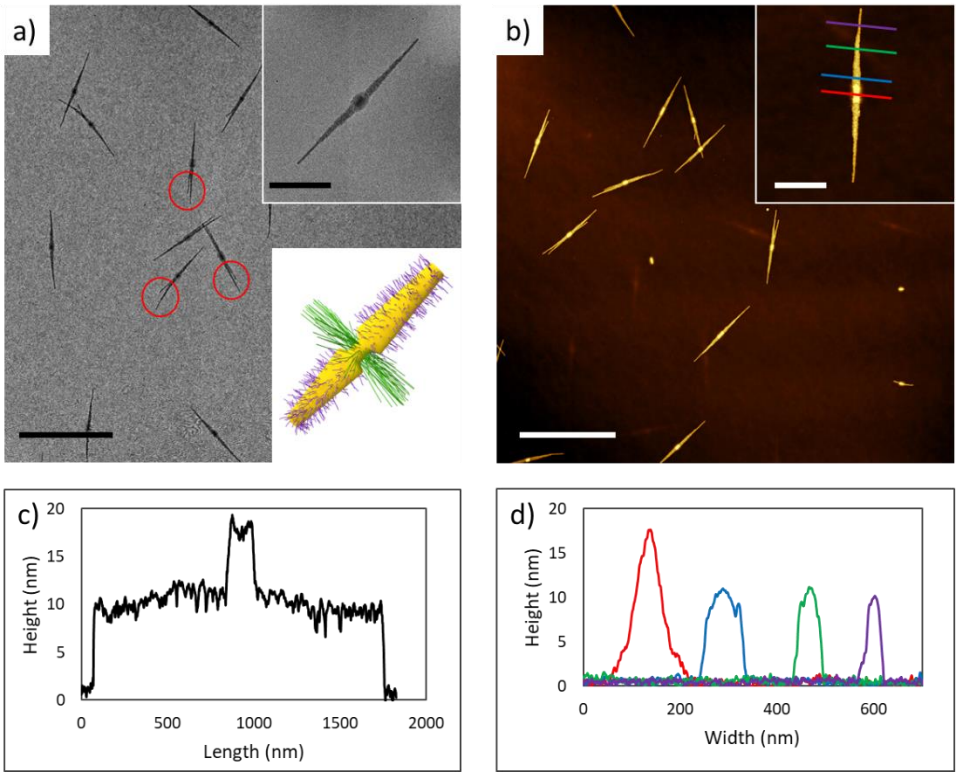

Figure 3. **(a)** TEM image with red circles indicating branching points of micelles and **(b)** AFM height image of tapered triblock co-micelles formed by seeded growth of **PFS$_{50}$-b-[PCE][AOT]$_{50}$** from **PFS$_{50}$-b-P2VP$_{739}$** seeds in *i*PrOH at a unimer:seed mass ratio of 15 at 21 °C after ageing for several months, **(c)** AFM height profile along length of micelle in inset of (b), **(d)** AFM height profiles of four sections along the triblock co-micelle. Scale bars = 2000 nm, insets = 500 nm. (For schematic inset in (a) green = P2VP, yellow = PFS and purple = [PCE][AOT]$_{50}$)

c) Self-assembly in a medium polarity medium (4:1 iPrOH:THF)

In order to improve the solubility of the unimer during the self-assembly process, molecularly dissolved **PFS$_{50}$-*b*-[PCE][AOT]$_{50}$** was added to **PFS$_{50}$-*b*-P2VP$_{739}$** seed micelles in 4:1 *i*PrOH:THF (as opposed to neat *i*PrOH used previously). As THF is a good solvent for both the PFS and [PCE][AOT]$_n$ blocks, solvent quality for the PFS-core forming block was improved using this mixed solvent system. At unimer:seed mass ratios of 5, 10 and 15, BAB triblock co-micelles

were observed by TEM after ageing overnight (Fig. 4a and S4). In contrast to the structures formed in *i*PrOH, neither pronounced tapering nor spherical micelles were evident. At a unimer:seed mass ratio of 15, the majority of micelles exhibited branching points in the terminal blocks; 66% of micelles had at least one branching point (Fig. 4a-c), a significantly higher degree than in *i*PrOH (37% of micelles). The number of branches on either side of the seed varied, ranging from one to three branches per terminal block (see Fig. S5 for distribution of number of branches per micelle).

AFM analysis showed that the terminal micelle segments (B), derived from **PFS$_{50}$-*b*-[PCE][AOT]$_{50}$** possessed a width near the seed interface of ca. 51 nm by AFM (Fig. 4c and d, blue trace, and S6), which is significantly less than for the tapered micelles in *i*PrOH (ca. 75 nm, Fig. 3d, blue trace). The width of a single branch (4:1 *i*PrOH:THF) (ca. 26 nm by AFM, Fig. 4d, green trace) is comparable to the width of the termini of the tapered structure (*i*PrOH) (ca. 24 nm, Fig. 3d, purple trace). In addition, the height of the terminal block is constant (ca. 10 nm, Fig. 4d) and corresponds closely to the height of the terminal blocks in the tapered micelles (ca. 10 nm, Fig. 3d).

As with the seeded growth in *i*PrOH, it was not possible to quantitatively calculate the increase in length of the micelles as the unimer:seed mass ratio increased, due to the branching. However, qualitatively, the terminal segments of the micelles increased in cumulative length (taking into account any branches present) by a factor of ca. 3 on increasing the unimer:seed mass ratio from 5 to 15 (Fig. 4 and S4).

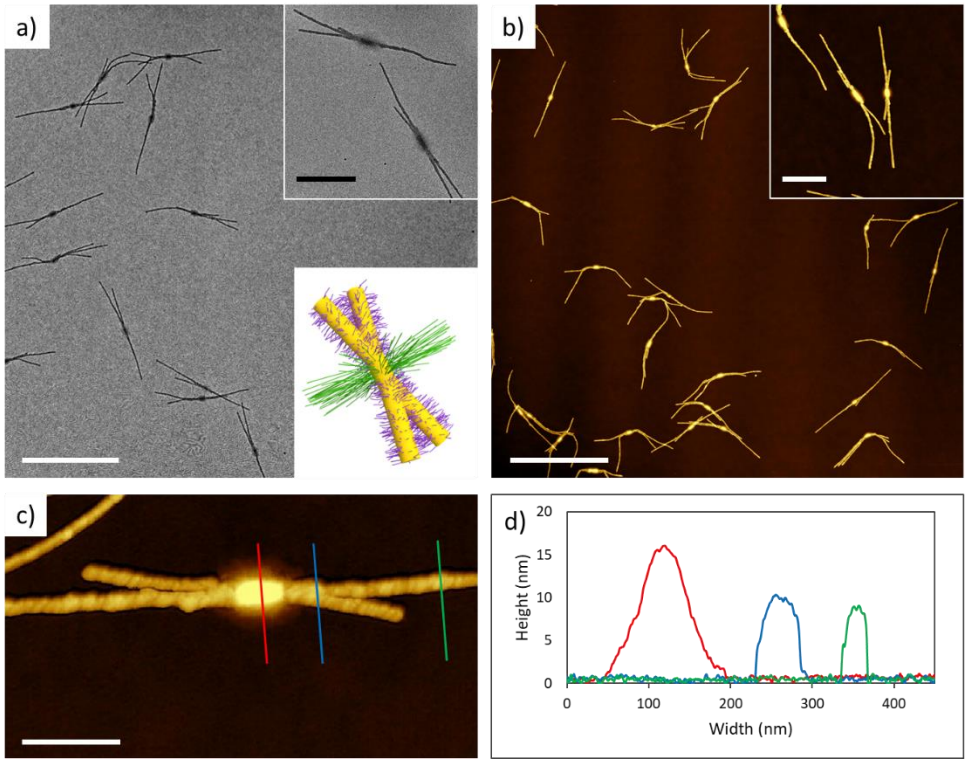

Figure 4. **(a)** TEM image and **(b)** AFM height image of branched triblock co-micelles formed by seeded growth of **PFS_{50}-b-[PCE][AOT]$_{50}$** from **PFS_{50}-b-$P2VP_{739}$** seeds in 4:1 *i*PrOH:THF at a unimer:seed mass ratio of 15 at 21 °C after ageing overnight, **(c)** Higher magnification of central section of a single micelle, with lines indicating where height profiles were measured, **(d)** Height profiles across sections of triblock co-micelle. Scale bars = (a and b) 2000 nm, (inset, a and b), 500 nm, (c) 200 nm. (For schematic inset in (a) green = P2VP, yellow = PFS and purple = $[PCE][AOT]_{50}$)

As the addition of 20% THF to the solvent mixture had a significant impact on the observed micelle morphology, we investigated whether changing the minority solvent from THF to other solvents would again lead to the formation of modified structures. The complementary solvent added to iPrOH was varied from non-polar aprotic *n*-hexane and diethyl ether (Et_2O) to more polar aprotic ethyl acetate (EtOAc) and polar protic MeOH, all of which are poor solvents for PFS. In

all self-assembly experiments (4:1 *i*PrOH:*n*-hexane, 4:1 *i*PrOH:Et_2O, 4:1 *i*PrOH:EtOAc, 4:1 *i*PrOH:MeOH) tapered structures were observed (Fig. S7), similar to the structures observed in pure *i*PrOH (Fig. 3), with kinetically trapped spheres particularly evident when hexane and diethyl ether were employed (Fig. S7b and c).

d) Effect of 'good solvent' content and temperature on micellar morphology

We also investigated whether the 1D micellar morphology could be altered by further varying the ratio of THF to *i*PrOH. **PFS_{50}-*b*-[PCE][AOT]$_{50}$** unimer solution in THF was added to 1D **PFS_{50}-*b*-$P2VP_{739}$** seeds in *i*PrOH:THF (at a constant unimer:seed mass ratio of 15), where the *i*PrOH:THF ratio of the seed solution was varied from 2:1 to 19:1. At the highest THF content of 2:1 *i*PrOH:THF, the majority (ca. 97%) of triblock micelles showed epitaxial 1D growth to form linear micelles with a width of 22 nm by TEM and no observable tapering or branching (Fig. 5a and see S8a for distribution of number of branches per micelle). As the THF content was reduced to 4:1 *i*PrOH:THF (as previously discussed in Section **b**), linear (ca. 34%) and branched (ca. 66%) structures were observed, where almost all branched structures had a maximum of two branches growing from any seed terminus (Fig. 5b and S8b). Decreasing the THF content further to 9:1 *i*PrOH:THF, tapering in the terminal blocks of the micelles became apparent (Fig. 5c). In addition, a small amount of the tapered micelles exhibited branching points in the terminal blocks (ca. 18%) (Fig. 5c and S8c). Reducing the THF content even further (19:1 *i*PrOH:THF) produced similar results to the experiment in 9:1 *i*PrOH:THF (Fig. 5d), in which tapering and a similar degree of branching was observed (Fig. S8d).

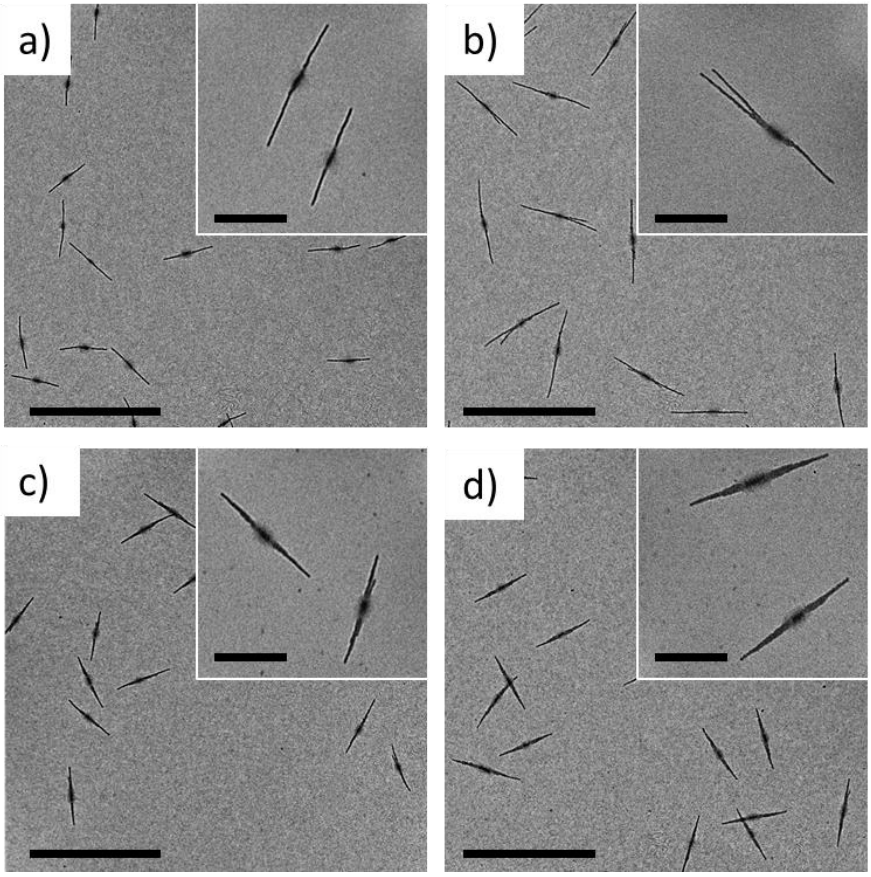

Figure 5. TEM images of triblock co-micelles formed by seeded growth of **PFS$_{50}$-b-[PCE][AOT]$_{50}$** from **PFS$_{50}$-b-P2VP$_{739}$** seeds in **(a)** 2:1 *i*PrOH:THF, **(b)** 4:1 *i*PrOH:THF, **(c)** 9:1 *i*PrOH:THF and **(d)** 19:1 *i*PrOH:THF at a unimer:seed mass ratio of 15 at 21 °C and aged overnight. Scale bars = 2000 nm, insets = 500 nm.

The effect of changing the self-assembly temperature from –16 to 21°C, and finally to 45 °C on the morphology of micelles obtained by seeded growth was also investigated. **PFS$_{50}$-*b*-[PCE][AOT]$_{50}$** unimer was added to **PFS$_{50}$-*b*-P2VP$_{739}$** seeds in both *i*PrOH and 4:1 *i*PrOH:THF at a variety of unimer:seed mass ratios. In *i*PrOH, upon increasing the temperature the width of the tapered structures reduced and fewer branching points per micelle occurred (Fig. S3, S9 and S10). In 4:1 *i*PrOH:THF a morphological change was apparent for the micelles on increasing temperature from tapered and branched, to linear (Fig. 6, S11–S13). The micelles formed by

seeded growth at –16 °C (unimer:seed mass ratio of 15) displayed branching and/or tapering, with several branches per micelle (Fig. 6a). Analysis of the TEM images showed that ca. 98 % of micelles formed at –16°C were branched (see Fig. S13a for distribution of branches per micelle). As the temperature was increased to room temperature (21 °C), fewer of the micelles exhibited branches (66%) (Fig. 6b and S13b). Upon heating to 45 °C during the seeded growth experiment, the degree of branching was further reduced (only ca. 18 % of the observed micelles exhibit branching), with the major product instead consisting of linear triblock co-micelles with no discernible tapering and a width of 26 nm by TEM (Fig. 6c and S13c).

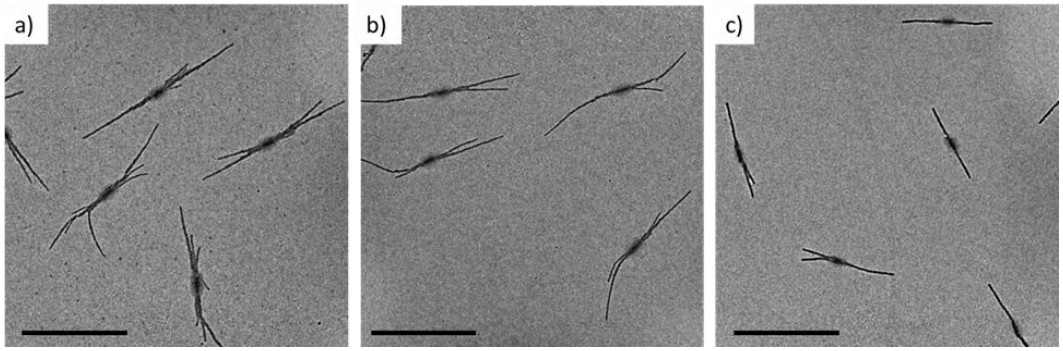

Figure 6. TEM images of triblock co-micelles formed by seeded growth of **PFS$_{50}$-b-[PCE][AOT]$_{50}$** from **PFS$_{50}$-b-P2VP$_{739}$** seeds in 4:1 *i*PrOH:THF at **(a)** –16 °C, **(b)** 21 °C and **(c)** 45 °C at a unimer:seed ratio of 15 and aged overnight. Scale bars = 1000 nm.

e) Seeded growth in a lower polarity medium (1:10 iPrOH:EtOAc)

Although at a solvent mixture of 2:1 *i*PrOH:THF linear triblock co-micelles were formed with consistent widths for the terminal blocks (i.e. no tapering), increasing THF content further can lead to the formation of 2D platelet structures.[61] To better solvate the PFS BCP unimer during self-assembly without using a large amount of THF, we changed the selective solvent from *i*PrOH:THF to a 1:10 *i*PrOH:EtOAc solvent mixture. Significantly, under these conditions seeded growth of **PFS$_{50}$-*b*-[PCE][AOT]$_{50}$** unimer from **PFS$_{50}$-*b*-P2VP$_{739}$** seeds in 1:10 *i*PrOH:EtOAc at 21 °C led

to 1D micelles with consistent widths along the terminal blocks, with no detectable tapering or branching (Fig. 7a, c-d), similar to those observed in seeded growth experiments in 2:1 *i*PrOH:THF. In neat EtOAc, micellar aggregates formed by seeded growth (Fig. S14 and S15), presumably due to the **PFS$_{50}$-*b*-P2VP$_{739}$** seeds aggregating prior to unimer addition, as P2VP is not well solvated by EtOAc. Seeded growth experiments in 1:10 *i*PrOH:EtOAc were carried out with a variety of unimer:seed mass ratios to investigate whether the length of the micelles could be precisely controlled. A linear correlation was evident between unimer:seed mass ratio and the L_n of the micelles (Fig. 7b), indicating that the growth of **PFS$_{50}$-*b*-[PCE][AOT]$_{50}$** unimer from **PFS$_{50}$-*b*-P2VP$_{739}$** seeds in 1:10 *i*PrOH:EtOAc is a living process (see Fig. S16–S21 for TEM images of micelles and histograms of micelle length distribution for various unimer:seed mass ratios).[14] AFM analysis showed that the height and width of the terminal block are consistent along its length, ca. 10 nm and 20 nm, respectively (Fig. 7e, blue and green trace), which are both substantially less than the values determined for the **PFS$_{50}$-*b*-P2VP$_{739}$** seed (Fig. 7e, red trace, height = 14 nm, width = 62 nm). These values correspond well to the height and width of the end of the tapered micelles (Fig. 3d, purple trace) and a single branch of the branched micelles (Fig. 4d, green trace).

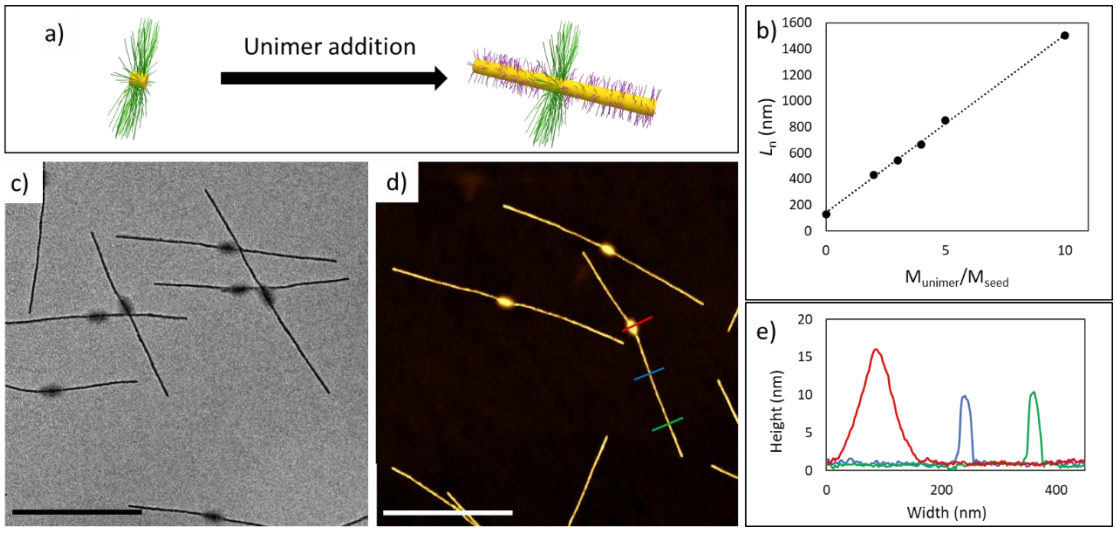

Figure 7. **(a)** Schematic showing seeded growth of **PFS$_{50}$-b-[PCE][AOT]$_{50}$** unimer from **PFS$_{50}$-b-P2VP$_{739}$** seeds, **(b)** Graph showing the average length (L_n) of triblock co-micelles vs. the unimer:seed mass ratio, **(c)** TEM image and **(d)** AFM height image of linear triblock co-micelles formed by seeded growth of **PFS$_{50}$-b-[PCE][AOT]$_{50}$** from **PFS$_{50}$-b-P2VP$_{739}$** seeds in 1:10 *i*PrOH:EtOAc at a unimer:seed mass ratio of 5 at 21 °C, after ageing overnight, **(e)** Height profiles across the central seed segment (red trace) and terminal block (blue and green traces) of a triblock co-micelle. Scale bars = 500 nm. (For schematic in (a) green = P2VP, yellow = PFS and purple = [PCE][AOT]$_{50}$)

Interestingly, unsymmetric growth in 1:10 *i*PrOH:EtOAc (i.e. more pronounced growth of terminal block from one terminus of the seed micelle compared to the other), was detected by TEM (Fig. 8). The unsymmetric growth was most pronounced at low unimer:seed mass ratios, but could still be observed in micelles over a micron in length, as the seed segment was not positioned in the centre of the triblock co-micelle. In an attempt to quantify the observed unsymmetric growth, the lengths of each terminal block were measured as well as the total length of the micelle for over 200 micelles by analysis of TEM images. At a unimer:seed mass ratio of 1, 63% of the resulting micelles showed no observable epitaxial growth from the seed, 30 % of the micelles exhibited growth from one of the two faces of the seeds, forming an AB-type micelle (where A is the seed block and B is the newly grown block) and in only 7% of the micelles was unimer addition to both faces of the seeds evident, to form the expected BAB-type micelle (Fig. 8a). On increasing the unimer:seed mass ratio to 2, this distribution was reversed in order, with no inactive seeds, 21% AB-type micelles and 79% BAB-type micelles (Fig. 8b). As the mass of unimer relative to the mass of seeds increased further, the number of seed faces with no unimer addition decreased until

at a unimer:seed mass ratio of 4, no inactive seeds, 3% AB-type and 97% BAB-type micelles were observed (Fig. 8d).

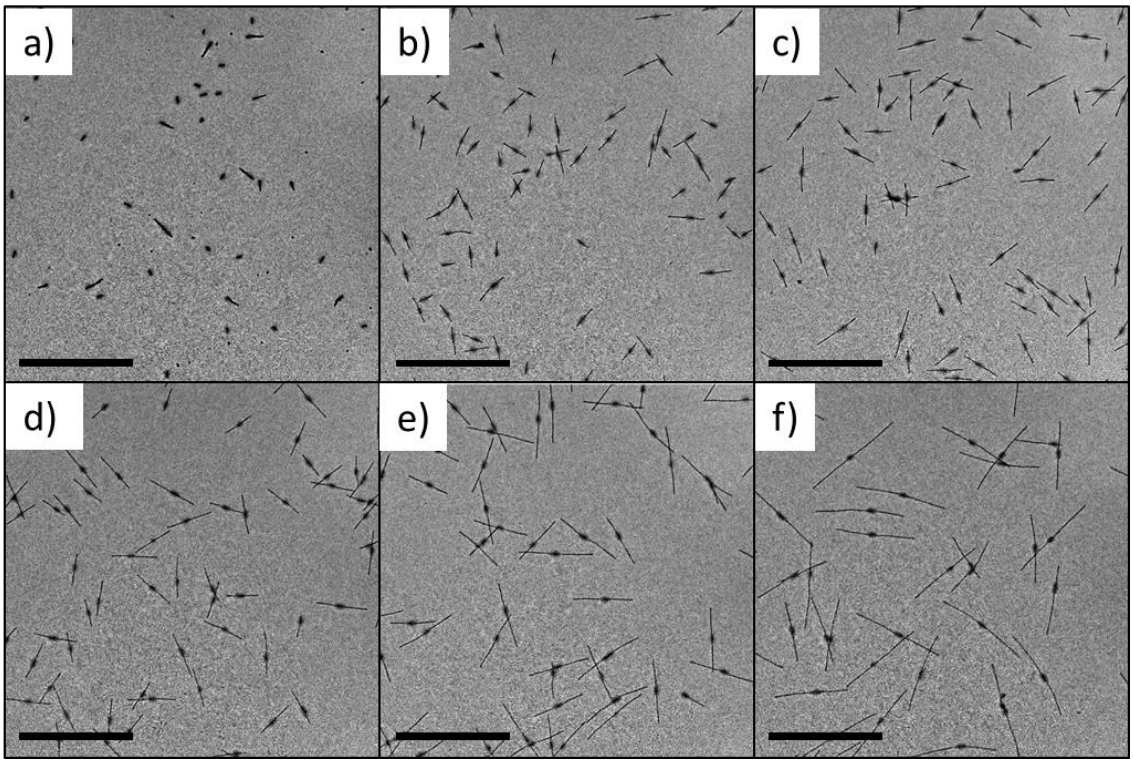

Figure 8. TEM images of linear triblock co-micelles formed by seeded growth of **PFS$_{50}$-b-[PCE][AOT]$_{50}$** from **PFS$_{50}$-b-P2VP$_{739}$** seeds in 1:10 *i*PrOH:EtOAc at unimer:seed mass ratios of **(a)** 1, **(b)** 2, **(c)** 3, **(d)** 4, **(e)** 5, **(f)** 10. Scale bars = 2000 nm.

Also of interest regarding the unsymmetric micelle growth was the difference in the lengths of the two terminal blocks of each triblock co-micelle and how this difference changed as the unimer:seed mass ratio increased. The length of both terminal blocks (L_x) per micelle, as well as the overall length of the micelle (L), were measured for all micelles (see Table 1). The difference between the lengths of the two terminal blocks on each micelle (ΔL_x) was calculated and divided by the total length of the micelle (L), then averaged for over 200 micelles. As the unimer:seed mass ratio increased from 2 to 5, the difference in length of the two terminal blocks (ΔL_x) remains

constant (ca. 90 nm, Table 1), even as the overall micelle length L did increase with unimer:seed mass ratio. The fact that ΔL_x remained relatively constant suggests that there is an initial lag to unimer addition to the seeds, which is independent of the unimer concentration. The data for unimer:seed mass ratio of 1 is anomalous due to a large percentage of seeds possessing no terminal block, meaning that ΔL_x is 0.

Table 1. **(a)** Schematic describing the values L and L_x for a linear triblock co-micelle, **(b)** table showing length parameters for micelles in 1:10 *i*PrOH:EtOAc at 21 °C. L is the length of the micelle, L_x is the length of the terminal block and ΔL_x is the difference in length between the terminal blocks per micelle. (For schematic in (a) green = P2VP, yellow = PFS and purple = [PCE][AOT]$_{50}$)

a) b)

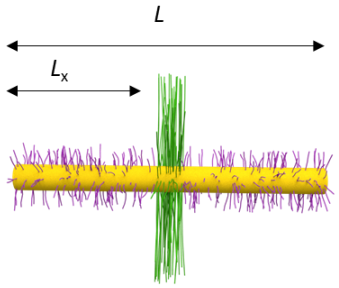

	U/S = 1	*U/S = 2*	*U/S = 3*	*U/S = 4*	*U/S = 5*
Average L	179	417	534	665	818
Average L_x	31	132	178	252	314
Average ΔL_x	48	97	87	82	93
Average $\Delta L_x/L$	0.16	0.24	0.18	0.14	0.12
% of seed termini with no elongation	78	11	4	2	0

f) Seeded growth using with seeds possessing different coronal chemistry

Having successfully formed triblock co-micelles in 1:10 *i*PrOH:EtOAc with a constant width along the terminal blocks (Fig. 7), we attempted the seeded growth of **PFS$_{50}$-*b*-[PCE][AOT]$_{50}$** unimer from seeds with coronas other than P2VP. It was possible to form linear triblock co-micelles in 1:10 *i*PrOH:EtOAc with both **PFS$_{46}$-*b*-PMVS$_{444}$** (PMVS = polymethylvinylsilane) and **PFS$_{53}$-*b*-(PEO-g-TEG)$_{136}$** (PEO = polyethyleneoxide, TEG = tetraethyleneglycol) seeds (Fig. S22-23 and S25-26 respectively). Growth from both seed samples

were living CDSA processes with good control over the length of the micelles (Fig. S24 and S27). Self-assembly of **PFS$_{50}$-*b*-[PCE][AOT]$_{50}$** in the absence of seeds via self-nucleation in acetone gave long fiber-like micelles that appear to aggregate on solvent removal (Fig. S28). Seeds could be formed from these **PFS$_{50}$-*b*-[PCE][AOT]$_{50}$** micelles by sonication, however subsequent addition of **PFS$_{50}$-*b*-[PCE][AOT]$_{50}$** unimer led to micelle growth with poor control over the length of the micelles (Fig. S28). It is expected that the [PCE][AOT] corona is not sufficiently well solvated to allow for controlled seeded growth. Future studies will aim to improve the colloidal stability of **PFS$_{50}$-*b*-[PCE][AOT]$_{50}$** seeds so that micelles containing exclusively **PFS$_{50}$-*b*-[PCE][AOT]$_{50}$** can be accessed.

The growth of **PFS$_{50}$-*b*-[PCE][AOT]$_{50}$** unimer from **PFS$_{53}$-b-(PEO-*g*-TEG)$_{136}$** seeds was also investigated in *i*PrOH and 4:1 *i*PrOH:THF (Fig. 9). As the seeds (Fig. 9a) did not possess high electron density coronas, it was expected that more insight could be gained into the structure of the triblock co-micelles at the interface between the seed and terminal blocks. Seeded growth in *i*PrOH at a unimer:seed mass ratio of 10 produced tapered structures (Fig. 9b), similar to those observed during seeded growth experiments with **PFS$_{50}$-*b*-P2VP$_{739}$** seeds. We assumed that only the metal-containing micelle cores of the assemblies were observable by TEM due to the high electron density. Measuring over 200 micelles in each sample by TEM, the widths of the seeds and the tapered structures were calculated to be 13 nm and 33 nm, respectively (the tapered micelles were measured at their widest points and the value decreased to 19 nm at the micelle termini). Growth in 4:1 *i*PrOH:THF also showed tapering, with wider micelle cores in the centre (Fig. 9c). However, the widths of the structures in 4:1 *i*PrOH:THF were measured to be 24 nm, less than the micelle widths in *i*PrOH. In both *i*PrOH and 4:1 *i*PrOH:THF the triblock co-micelles were wider than the seeds they grew from.

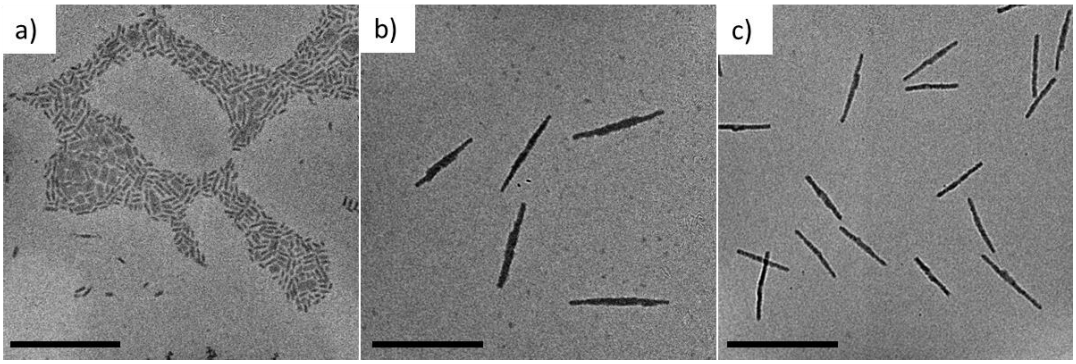

Figure 9. TEM images of **(a) PFS$_{46}$-b-(PEO-g-TEG)$_{156}$** seed micelles, L_n = 35 nm and triblock co-micelles formed by seeded growth of **PFS$_{50}$-b-[PCE][AOT]$_{50}$** from **PFS$_{53}$-b-(PEO-g-TEG)$_{136}$** seeds in **(b)** *i*PrOH and **(c)** 4:1 *i*PrOH:THF. Scale bars = 500 nm. The seed micelles in **(a)** possess a significant population of platelet impurities. These were not found to affect subsequent seeded growth (see Fig. S25-27) and are therefore presumably insoluble in the solvent medium used.

g) Counter-Ion Exchange

Next, we investigated whether the surfactant counter-anion could be replaced by a halide after self-assembly had taken place, in order to produce micelles that would be colloidally stable in aqueous media. The possibility of changing the counterion of the $[PCE]^{n+}$ corona offers an attractive opportunity to alter the chemical functionality and solubility of the micelles simply and modularly. It should also be possible to form micelles that would not have been possible by seeded growth due to the insolubility of the required unimers.

The AOT surfactant was exchanged for a bromide anion (Br^-), as $[PCE][Br]_n$ homopolymers are known to be readily soluble in water.[34] After ageing for 16 h, large uncontrolled aggregates of fiber-like micelles could be detected by TEM (Fig. 10b). We believe this is due to the newly formed $[PCE][Br]_n$ corona being insoluble in the organic solvent mixture. Upon addition of excess water, the micelles re-dispersed (Fig. 10c), however dialysis to remove excess salt caused significant fragmentation of the micelles (Fig. S29), potentially due to interaction of the

polyelectrolyte corona with the dialysis tubing. An alternative possibility based on a recent report is that the fragmentation of micelles occurs due to an increase in osmotic pressure on addition of water.[28] It is envisaged that a range of functional counterions could be complexed to the polyelectrolytic $[PCE]^{n+}$ corona block and, with careful solvent selection, these could be re-dispersed post complexation.

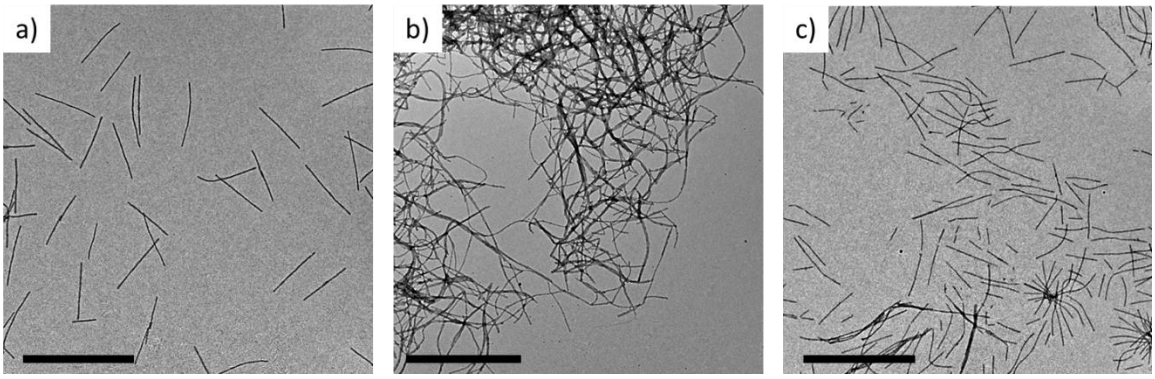

Figure 10. TEM images of **(a)** triblock co-micelles formed by seeded growth of **PFS$_{50}$-b-[PCE][AOT]$_{50}$** from **PFS$_{53}$-b-(PEO-g-TEG)$_{136}$** seeds in 1:10 *i*PrOH:EtOAc at a unimer:seed mass ratio of 50 at 21 °C, diluted in iPrOH to give a final solvent composition of 1:1 *i*PrOH:EtOAc, **(b)** triblock co-micelles M(**PFS$_{50}$-b-[PCE][Br]$_{50}$**)-b-M(**PFS$_{53}$-b-(PEO-g-TEG)$_{136}$**)-b-M(**PFS$_{50}$-b-[PCE][Br]$_{50}$**) in 1:1 *i*PrOH:EtOAc, **(c)** triblock co-micelles M(**PFS$_{50}$-b-[PCE][Br]$_{50}$**)-b-M(**PFS$_{53}$-b-(PEO-g-TEG)$_{136}$**)-b-M(**PFS$_{50}$-b-[PCE][Br]$_{50}$**) in 8:1:1 water:*i*PrOH:EtOAc. Scale bars = 2000 nm.

Discussion

We have examined the self-assembly of **PFS$_{50}$-*b*-[PCE][AOT]$_{50}$** under numerous seeded growth conditions. PFS BCPs with a 1:1 degree of polymerization ratio of the core- to corona-forming blocks usually form 2D micelles.[64] In the present study, addition of **PFS$_{50}$-b-[PCE][AOT]$_{50}$** unimer to seed micelles always led to generation of 1D micelles despite the 1:1 block ratio. We attribute this difference to the large effective volume of the solvent-swollen coronal block that

includes a substantial contribution from the AOT anions. The combination of these factors would be expected to favor a high degree of curvature of the core-corona interface and to therefore yield 1D rather than 2D assemblies.

In polar solvents, such as *i*PrOH, PFS is very poorly solvated (Hildebrand solubility parameters; δ_{PFS} = 18.7 $MPa^{1/2}$, δ_{iPrOH} = 23.8 $MPa^{1/2}$). Under these conditions presumably some precipitation of the **PFS$_{50}$** segment in the **PFS$_{50}$-*b*-[PCE][AOT]$_{50}$** unimers as kinetically trapped spheres with an amorphous PFS core occurs before the seed termini are encountered (Fig. S3), which is consistent with previous results in the literature.[53, 61, 65] In addition, the formation of tapered structures (Fig. 3) was detected under these seeded growth conditions. Initially, the seed appears to induce cylinder elongation in which the newly grown region is of similar width (but of reduced height) compared to the **PFS$_{50}$-b-P2VP$_{739}$** seeds. As the terminal blocks consisting of **PFS$_{50}$-*b*-[PCE][AOT]$_{50}$** grow further, the micelle core width reduces, producing a distinct tapering effect. It is expected that a higher degree of chain folding would reduce the areal density of the swollen [PCE][AOT] coronas, which have a large effective volume and potentially also Coulombic repulsions.[22] This increase in the degree of chain folding would lead to micelle cores with narrower widths. The formation of branched structures under slightly different solvent conditions can also be explained by the preference for high degrees of chain folding of **PFS$_{50}$-*b*-[PCE][AOT]$_{50}$**, which allows multiple cylinders of lower width to grow from the exposed faces at the end of the seed micelles (Fig. 4c).[22] In contrast, at elevated temperature, or in solvent media that are less poor for PFS such as *i*PrOH containing substantial amounts of THF (δ_{THF} = 18.5 $MPa^{1/2}$) or EtOAc (δ_{EtOAc} = 18.2 $MPa^{1/2}$) linear cylinders of uniform width are formed rather than branched or tapered structures. In these cases the formation of a uniform, chain-folded core is probably favored by the reduced rate of crystallization-driven growth.[22, 66] Previously, ABC miktoarm star polymers were

shown to undergo self-assembly yielding a variety of morphologies as a function of the pH of the self-assembly solution.[67]

Surprisingly, addition of **PFS$_{50}$-*b*-[PCE][AOT]$_{50}$** unimer to **PFS$_{50}$-*b*-P2VP$_{739}$** seeds in 1:10 *i*PrOH:EtOAc led to block co-micelles that exhibited unsymmetrical growth, i.e. the growth of the terminal block from one of the seed termini was more pronounced than from the other (Fig. 8). This suggests that the initial addition of the unimer to a seed terminus is disfavored. This behavior may be a consequence of the very long, swollen P2VP block (δ_{P2VP} = 20.6 MPa$^{1/2}$)[68] present in the seeds, which would be expected to produce a steric barrier to incoming unimer as it approaches the faces at the seed termini. Following successful but slow addition to one face of the seed, the steric barrier to further unimer addition at this site would be reduced as the terminus on the elongated micelle becomes more distant from the P2VP seed corona. Consistent with this explanation, at lower unimer:seed mass ratios, the barrier caused by the long P2VP corona blocking access to the crystal faces at the seed termini leads to a large proportion of unimer addition to relatively few seed faces, producing a mixture of BAB-type micelles, AB-type micelles and seeds. Only at a unimer:seed mass ratio of 5 is there unimer addition to all of the seed micelle termini (Fig. 8 and Table 1). The concentration of unimer is higher and therefore the frequency of unimer encountering seed termini is expected to increase, leading to solely triblock co-micelles. Interestingly, even at high unimer:seed mass ratios, the difference in length of the terminal blocks remains (Fig. 8d-f), suggesting that the effects of the unfavorable initial unimer addition step is still present.

Conclusions

We have studied the CDSA of a heterobimetallic BCP polyelectrolyte/surfactant complex, **PFS$_{50}$-*b*-[PCE][AOT]$_{50}$**. Seeded growth was possible and the resulting micellar morphology

(linear, branched or tapered) could be varied by changing the solvent conditions or the temperature. The experimental conditions presumably affect the solubility of the PFS unimer and hence the speed of deposition and crystallisation onto the faces of the seed termini. Under poorly solvated conditions tapered and branched structures were formed and further work is needed to understand the subtle factors that influence the morphologies formed. On increasing the solubility of the PFS unimer, deposition occurred in a more controlled manner leading to the formation of linear micellar structures. Colloidally stable micelles with a charged corona are of interest for the potential of loading with functional cargoes, as well as their possible interactions with oppositely charged surfaces or colloids.

Seeded growth experiments in 1:10 *i*PrOH:EtOAc at a unimer:seed ratio 1:1 produced a mixture of seeds with no unimer added, seeds with unimer addition on one face (AB-type micelles), and seeds with unimer addition on both faces (BAB-type micelles). We postulate that initial addition of the unimer to the seeds is sterically hindered by the long, solvent swollen P2VP corona of the seeds blocking the faces of the seed termini. At larger unimer:seed ratios unimer addition to all the faces of the seed termini occurred, however unsymmetric growth was still observed.

Post self-assembly exchange of the $[AOT]^-$ surfactant for an Br^- counteranion dramatically altered the solubility of the micelles, leading to aggregation in organic solvents. However, on addition of water, the micelles could be re-dispersed. This offers an attractive opportunity to chemically modify the corona post self-assembly in a manner that does not affect the morphology of the micelle and further exploration of this approach is in progress.

ASSOCIATED CONTENT

Supporting Information. Is available containing details of the synthesis, self-assembly experiments and additional TEM images.

AUTHOR INFORMATION

Corresponding Author

*Ian Manners (imanners@uvic.ca), *Charl F. J. Faul (charl.faul@bristol.ac.uk).

Funding Sources

C. J.-W. thanks the Bristol Chemical Synthesis Centre for Doctoral Training, funded by the Engineering and Physical Sciences Research Council (EPSRC) for PhD funding (EP/G036764/1). Mass spectrometric analysis was performed on instrumentation bought through the Core Capability for Chemistry Research - Strategic Investment in Mass Spectrometry EPSRC grant (EP/K03927X/1). PeakForce atomic force microscopy was carried out in the Chemical Imaging Facility, University of Bristol with equipment funded by EPSRC under "Atoms to Applications" Grant EP/K035746/1. I.M. thanks the University of Bristol for support and the Canadian Government of a Canada 150 Research Chair.

REFERENCES

1. Tritschler, U.; Pearce, S.; Gwyther, J.; Whittell, G. R.; Manners, I., 50th Anniversary Perspective: Functional Nanoparticles from the Solution Self-Assembly of Block Copolymers. *Macromolecules* **2017,** *50*, 3439-3463.
2. Du, Z.-X.; Xu, J.-T.; Fan, Z.-Q., Micellar Morphologies of Poly(ε-caprolactone)-b-poly(ethylene oxide) Block Copolymers in Water with a Crystalline Core. *Macromolecules* **2007,** *40*, 7633-7637.
3. Wang, X.; Guerin, G.; Wang, H.; Wang, Y.; Manners, I.; Winnik, M. A., Cylindrical Block Copolymer Micelles and Co-Micelles of Controlled Length and Architecture. *Science* **2007,** *317*, 644-647.
4. Lee, E.; Hammer, B.; Kim, J.-K.; Page, Z.; Emrick, T.; Hayward, R. C., Hierarchical Helical Assembly of Conjugated Poly(3-hexylthiophene)-block-poly(3-triethylene glycol thiophene) Diblock Copolymers. *J. Am. Chem. Soc.* **2011,** *133*, 10390-10393.
5. Schmelz, J.; Schedl, A. E.; Steinlein, C.; Manners, I.; Schmalz, H., Length Control and Block-Type Architectures in Worm-like Micelles with Polyethylene Cores. *J. Am. Chem. Soc.* **2012,** *134*, 14217-14225.
6. He, W.-N.; Xu, J.-T., Crystallization assisted self-assembly of semicrystalline block copolymers. *Prog. Polym. Sci.* **2012,** *37*, 1350-1400.
7. Schöbel, J.; Karg, M.; Rosenbach, D.; Krauss, G.; Greiner, A.; Schmalz, H., Patchy Wormlike Micelles with Tailored Functionality by Crystallization-Driven Self-Assembly: A Versatile Platform for Mesostructured Hybrid Materials. *Macromolecules* **2016,** *49*, 2761-2771.
8. Foster, J. C.; Varlas, S.; Couturaud, B.; Coe, Z.; O'Reilly, R. K., Getting into Shape: Reflections on a New Generation of Cylindrical Nanostructures' Self-Assembly Using Polymer Building Blocks. *J. Am. Chem. Soc.* **2019,** *141*, 2742-2753.
9. Wang, J.; Lu, Y.; Chen, Y., Fabrication of 2D surface-functional polymer platelets via crystallization-driven self-assembly of poly(ε-caprolactone)-contained block copolymers. *Polymer* **2019,** *160*, 196-203.
10. Yin, L.; Hillmyer, M. A., Disklike Micelles in Water from Polyethylene-Containing Diblock Copolymers. *Macromolecules* **2011,** *44*, 3021-3028.
11. Xu, F.; Zhang, P.; Zhang, J.; Yu, C.; Yan, D.; Mai, Y., Crystallization-Driven Two-Dimensional Self-Assembly of Amphiphilic PCL-b-PEO Coated Gold Nanoparticles in Aqueous Solution. *ACS Macro Lett.* **2018,** *7*, 1062-1067.
12. Han, L.; Wang, M.; Jia, X.; Chen, W.; Qian, H.; He, F., Uniform two-dimensional square assemblies from conjugated block copolymers driven by π–π interactions with controllable sizes. *Nat. Commun.* **2018,** *9*, 865.
13. Ganda, S.; Dulle, M.; Drechsler, M.; Förster, B.; Förster, S.; Stenzel, M. H., Two-Dimensional Self-Assembled Structures of Highly Ordered Bioactive Crystalline-Based Block Copolymers. *Macromolecules* **2017,** *50*, 8544-8553.
14. Gilroy, J. B.; Gadt, T.; Whittell, G. R.; Chabanne, L.; Mitchels, J. M.; Richardson, R. M.; Winnik, M. A.; Manners, I., Monodisperse cylindrical micelles by crystallization-driven living self-assembly. *Nat. Chem.* **2010,** *2*, 566-70.
15. Petzetakis, N.; Dove, A. P.; O'Reilly, R. K., Cylindrical micelles from the living crystallization-driven self-assembly of poly(lactide)-containing block copolymers. *Chem. Sci.* **2011,** *2*, 955-960.

16. Shin, S.; Menk, F.; Kim, Y.; Lim, J.; Char, K.; Zentel, R.; Choi, T.-L., Living Light-Induced Crystallization-Driven Self-Assembly for Rapid Preparation of Semiconducting Nanofibers. *J. Am. Chem. Soc.* **2018,** *140*, 6088-6094.
17. Qiu, H.; Gao, Y.; Boott, C. E.; Gould, O. E. C.; Harniman, R. L.; Miles, M. J.; Webb, S. E. D.; Winnik, M. A.; Manners, I., Uniform patchy and hollow rectangular platelet micelles from crystallizable polymer blends. *Science* **2016,** *352*, 697-701.
18. Mai, Y.; Eisenberg, A., Self-assembly of block copolymers. *Chem. Soc. Rev.* **2012,** *41*, 5969-85.
19. Hailes, R. L. N.; Oliver, A. M.; Gwyther, J.; Whittell, G. R.; Manners, I., Polyferrocenylsilanes: Synthesis, Properties, and Applications. *Chem. Soc. Rev.* **2016,** *45*, 5358-5407.
20. Gädt, T.; Ieong, N. S.; Cambridge, G.; Winnik, M. A.; Manners, I., Complex and hierarchical micelle architectures from diblock copolymers using living, crystallization-driven polymerizations. *Nat. Mater.* **2009,** *8*, 144-50.
21. Qiu, H.; Du, V. A.; Winnik, M. A.; Manners, I., Branched cylindrical micelles via crystallization-driven self-assembly. *J. Am. Chem. Soc.* **2013,** *135*, 17739-42.
22. Qiu, H.; Gao, Y.; Du, V. A.; Harniman, R.; Winnik, M. A.; Manners, I., Branched Micelles by Living Crystallization-Driven Block Copolymer Self-Assembly under Kinetic Control. *J. Am. Chem. Soc.* **2015,** *137*, 2375-2385.
23. Hudson, Z. M.; Boott, C. E.; Robinson, M. E.; Rupar, P. A.; Winnik, M. A.; Manners, I., Tailored hierarchical micelle architectures using living crystallization-driven self-assembly in two dimensions. *Nat. Chem.* **2014,** *6*, 893-898.
24. Yu, B.; Jiang, X.; Yin, J., Size-Tunable Nanosheets by the Crystallization-Driven 2D Self-Assembly of Hyperbranched Poly(ether amine) (hPEA). *Macromolecules* **2014,** *47*, 4761-4768.
25. Li, X.; Gao, Y.; Boott, C. E.; Winnik, M. A.; Manners, I., Non-covalent synthesis of supermicelles with complex architectures using spatially confined hydrogen-bonding interactions. *Nat. Commun.* **2015,** *6*, 8127.
26. Hudson, Z. M.; Lunn, D. J.; Winnik, M. A.; Manners, I., Colour-tunable fluorescent multiblock micelles. *Nat. Commun.* **2014,** *5*, 3372.
27. Lunn, D. J.; Gould, O. E. C.; Whittell, G. R.; Armstrong, D. P.; Mineart, K. P.; Winnik, M. A.; Spontak, R. J.; Pringle, P. G.; Manners, I., Microfibres and macroscopic films from the coordination-driven hierarchical self-assembly of cylindrical micelles. *Nat. Commun.* **2016,** *7*, 12371.
28. Arno, M. C.; Inam, M.; Coe, Z.; Cambridge, G.; Macdougall, L. J.; Keogh, R.; Dove, A. P.; O'Reilly, R. K., Precision Epitaxy for Aqueous 1D and 2D Poly(ε-caprolactone) Assemblies. *J. Am. Chem. Soc.* **2017,** *139*, 16980-16985.
29. Choi, I.; Yang, S.; Choi, T.-L., Preparing Semiconducting Nanoribbons with Tunable Length and Width via Crystallization-Driven Self-Assembly of a Simple Conjugated Homopolymer. *J. Am. Chem. Soc.* **2018,** *140*, 17218-17225.
30. Qian, J.; Li, X.; Lunn, D. J.; Gwyther, J.; Hudson, Z. M.; Kynaston, E.; Rupar, P. A.; Winnik, M. A.; Manners, I., Uniform, High Aspect Ratio Fiber-like Micelles and Block Co-micelles with a Crystalline π-Conjugated Polythiophene Core by Self-Seeding. *J. Am. Chem. Soc.* **2014,** *136*, 4121-4124.
31. Jin, X.-H.; Price, M. B.; Finnegan, J. R.; Boott, C. E.; Richter, J. M.; Rao, A.; Menke, S. M.; Friend, R. H.; Whittell, G. R.; Manners, I., Long-range exciton transport in conjugated polymer nanofibers prepared by seeded growth. *Science* **2018,** *360*, 897-900.

32. Mayer, U. F. J.; Gilroy, J. B.; O'Hare, D.; Manners, I., Ring-opening polymerization of 19-electron [2]cobaltocenophanes: A route to high-molecular-weight, water-soluble polycobaltocenium polyelectrolytes. *J. Am. Chem. Soc.* **2009,** *131*, 10382-10383.
33. Mayer, U. F. J.; Charmant, J. P. H.; Rae, J.; Manners, I., Synthesis and Structures of Strained, Neutral [d7] and Cationic [d6] Hydrocarbon-Bridged [n]Cobaltocenophanes (n = 2, 3). *Organometallics* **2008,** *27*, 1524-1533.
34. Zhang, J.; Chen, Y. P.; Miller, K. P.; Ganewatta, M. S.; Bam, M.; Yan, Y.; Nagarkatti, M.; Decho, A. W.; Tang, C., Antimicrobial Metallopolymers and Their Bioconjugates with Conventional Antibiotics against Multidrug-Resistant Bacteria. *J. Am. Chem. Soc.* **2014,** *136*, 4873-4876.
35. Yan, Y.; Zhang, J.; Ren, L.; Tang, C., Metal-containing and related polymers for biomedical applications. *Chem. Soc. Rev.* **2016,** *45*, 5232-5263.
36. Zhang, J.; Yan, J.; Pageni, P.; Yan, Y.; Wirth, A.; Chen, Y.-P.; Qiao, Y.; Wang, Q.; Decho, A. W.; Tang, C., Anion-Responsive Metallopolymer Hydrogels for Healthcare Applications. *Sci. Rep.* **2015,** *5*, 11914.
37. Ganewatta, M. S.; Tang, C., Controlling macromolecular structures towards effective antimicrobial polymers. *Polymer* **2015,** *63*, A1-A29.
38. Wang, Y. L.; Rapakousiou, A.; Astruc, D., ROMP Synthesis of Cobalticenium-Enamine Polyelectrolytes. *Macromolecules* **2014,** *47*, 3767-3774.
39. Rapakousiou, A.; Wang, Y. L.; Belin, C.; Pinaud, N.; Ruiz, J.; Astruc, D., 'Click' Synthesis and Redox Properties of Triazolyl Cobalticinium Dendrimers. *Inorg. Chem.* **2013,** *52*, 6685-6693.
40. Gu, H.; Ciganda, R.; Castel, P.; Moya, S.; Hernandez, R.; Ruiz, J.; Astruc, D., Tetrablock Metallopolymer Electrochromes. *Angew. Chem. Int. Ed.* **2018,** *57*, 2204-2208.
41. Gu, H.; Ciganda, R.; Castel, P.; Ruiz, J.; Astruc, D., Living ROMP Synthesis and Redox Properties of Triblock Metallocopolymers Containing Side-Chain Iron and Cobalt Sandwich Complexes. *Macromol. Chem. Phys.* **2018,** *219*, 1800384.
42. Cuadrado, I.; Casado, C. M.; Lobete, F.; Alonso, B.; González, B.; Losada, J.; Amador, U., Preparation and Redox Properties of Novel Polymerizable Pyrrole- and Allyl-Functionalized Cobaltocenium Monomers and Siloxane-Based Cobaltocenium Polymers. *Organometallics* **1999,** *18*, 4960-4969.
43. Kenawy, E.-R.; Worley, S. D.; Broughton, R., The Chemistry and Applications of Antimicrobial Polymers: A State-of-the-Art Review. *Biomacromolecules* **2007,** *8*, 1359-1384.
44. Antonietti, M.; Conrad, J., Synthesis of Very Highly Ordered Liquid Crystalline Phases by Complex Formation of Polyacrylic Acid with Cationic Surfactants. *Angew. Chem. Int. Ed.* **1994,** *33*, 1869-1870.
45. Zhou, S.; Chu, B., Assembled Materials: Polyelectrolyte–Surfactant Complexes. *Adv. Mater.* **2000,** *12*, 545-556.
46. Lindman, B.; Antunes, F.; Aidarova, S.; Miguel, M.; Nylander, T., Polyelectrolyte-surfactant association—from fundamentals to applications. *Colloid J+* **2014,** *76*, 585-594.
47. von Ferber, C.; Lowen, H., Polyelectrolyte-surfactant complex: phases of self-assembled structures. *Faraday Discussions* **2005,** *128*, 389-405.
48. Faul, C. F. J.; Antonietti, M., Ionic Self-Assembly: Facile Synthesis of Supramolecular Materials. *Adv. Mater.* **2003,** *15*, 673-683.
49. Faul, C. F. J., Ionic Self-Assembly for Functional Hierarchical Nanostructured Materials. *Acc. Chem. Res.* **2014,** *47*, 3428-3438.

50. Ahmed, R.; Patra, S. K.; Hamley, I. W.; Manners, I.; Faul, C. F. J., Tetragonal and Helical Morphologies from Polyferrocenylsilane Block Polyelectrolytes via Ionic Self-Assembly. *J. Am. Chem. Soc.* **2013,** *135*, 2455-2458.
51. Ahmed, R.; Hsiao, M.-S.; Matsuura, Y.; Houbenov, N.; Faul, C. F. J.; Manners, I., Redox-active mesomorphic complexes from the ionic self-assembly of cationic polyferrocenylsilane polyelectrolytes and anionic surfactants. *Soft Matter* **2011,** *7*, 10462-10471.
52. Musgrave, R. A.; Choi, P.; Harniman, R. L.; Richardson, R. M.; Shen, C.; Whittell, G. R.; Crassous, J.; Qiu, H.; Manners, I., Chiral Transmission to Cationic Polycobaltocenes over Multiple Length Scales Using Anionic Surfactants. *J. Am. Chem. Soc.* **2018,** *140*, 7222-7231.
53. Gilroy, J. B.; Patra, S. K.; Mitchels, J. M.; Winnik, M. A.; Manners, I., Main-chain heterobimetallic block copolymers: synthesis and self-assembly of polyferrocenylsilane-b-poly(cobaltoceniumethylene). *Angew. Chem. Int. Ed.* **2011,** *50*, 5851-5.
54. Wang, X.; Winnik, M. A.; Manners, I., Synthesis and Self-Assembly of Poly(ferrocenyldimethylsilane-b-dimethylaminoethyl methacrylate): Toward Water-Soluble Cylinders with an Organometallic Core. *Macromolecules* **2005,** *38*, 1928-1935.
55. Gonzalez-Alvarez, M. J.; Jia, L.; Guerin, G.; Kim, K. S.; An Du, V.; Walker, G.; Manners, I.; Winnik, M. A., How a Small Modification of the Corona-Forming Block Redirects the Self-Assembly of Crystalline–Coil Block Copolymers in Solution. *Macromolecules* **2016,** *49*, 7975-7984.
56. Wang, H.; Lin, W. J.; Fritz, K. P.; Scholes, G. D.; Winnik, M. A.; Manners, I., Cylindrical block co-micelles with spatially selective functionalization by nanoparticles. *J. Am. Chem. Soc.* **2007,** *129*, 12924-12925.
57. Shusharina, N. P.; Nyrkova, I. A.; Khokhlov, A. R., Diblock Copolymers with a Charged Block in a Selective Solvent: Micellar Structure. *Macromolecules* **1996,** *29*, 3167-3174.
58. Odijk, T., Polyelectrolytes near the rod limit. *Journal of Polymer Science: Polymer Physics Edition* **1977,** *15*, 477-483.
59. Skolnick, J.; Fixman, M., Electrostatic Persistence Length of a Wormlike Polyelectrolyte. *Macromolecules* **1977,** *10*, 944-948.
60. For recent work on the formation of 2D assemblies from polycaprolactone BCPs with a coronal block containing cobaltocenium side groups see: Cha, Y.; Jarrett-Wilkins, C.; Rahman, M. A.; Zhu, T.; Sha, Y.; Manners, I.; Tang, C. Crystallization-Driven Self-Assembly of Metallo-Polyelectrolyte Block Copolymers with a Polycaprolactone Core-Forming Segment *ACS Macro Lett.* **2019** online DOI: 10.1021/acsmacrolett.9b00335.
61. Hsiao, M.-S.; Yusoff, S. F. M.; Winnik, M. A.; Manners, I., Crystallization-Driven Self-Assembly of Block Copolymers with a Short Crystallizable Core-Forming Segment: Controlling Micelle Morphology through the Influence of Molar Mass and Solvent Selectivity. *Macromolecules* **2014,** *47*, 2361-2372.
62. Keller, A.; Cheng, S. Z. D., The role of metastability in polymer phase transitions. *Polymer* **1998,** *39*, 4461-4487.
63. Jain, S.; Bates, F. S., Consequences of Nonergodicity in Aqueous Binary PEO−PB Micellar Dispersions. *Macromolecules* **2004,** *37*, 1511-1523.
64. Cao, L.; Manners, I.; Winnik, M. A., Influence of the Interplay of Crystallization and Chain Stretching on Micellar Morphologies: Solution Self-Assembly of Coil−Crystalline Poly(isoprene-block-ferrocenylsilane). *Macromolecules* **2002,** *35*, 8258-8260.

65. Wang, H.; Winnik, M. A.; Manners, I., Synthesis and Self-Assembly of Poly(ferrocenyldimethylsilane-b-2-vinylpyridine) Diblock Copolymers. *Macromolecules* **2007,** *40*, 3784-3789.
66. Boott, C. E.; Leitao, E. M.; Hayward, D. W.; Laine, R. F.; Mahou, P.; Guerin, G.; Winnik, M. A.; Richardson, R. M.; Kaminski, C. F.; Whittell, G. R.; Manners, I., Probing the Growth Kinetics for the Formation of Uniform 1D Block Copolymer Nanoparticles by Living Crystallization-Driven Self-Assembly. *ACS Nano* **2018,** *12*, 8920-8933.
67. Xu, F.; Wu, D.; Huang, Y.; Wei, H.; Gao, Y.; Feng, X.; Yan, D.; Mai, Y., Multi-Dimensional Self-Assembly of a Dual-Responsive ABC Miktoarm Star Terpolymer. *ACS Macro Lett.* **2017,** *6*, 426-430.
68. Jeong, J. W.; Park, W. I.; Kim, M.-J.; Ross, C. A.; Jung, Y. S., Highly Tunable Self-Assembled Nanostructures from a Poly(2-vinylpyridine-b-dimethylsiloxane) Block Copolymer. *Nano Letters* **2011,** *11*, 4095-4101.